BABAR-CONF-02/030
SLAC-PUB-9305
hep-ex/0207080
July 2002

Measurement of the CKM Matrix Element $|V_{ub}|$ with Charmless Exclusive Semileptonic B Meson Decays at *BABAR*

The *BABAR* Collaboration

July 25, 2002

Abstract

We present a preliminary measurement of the branching fraction for $B \to \rho e \nu$ and of the CKM matrix element $|V_{ub}|$ using approximately 55 million $B\bar{B}$ meson pairs collected with the *BABAR* detector. Using isospin relations for several modes we find

$$\begin{aligned} \mathcal{B}(B^0 \to \rho^- e^+ \nu) &= (3.39 \pm 0.44 \pm 0.52 \pm 0.60) \times 10^{-4} \\ |V_{ub}| &= (3.69 \pm 0.23 \pm 0.27\ ^{+0.40}_{-0.59}) \times 10^{-3}. \end{aligned}$$

The quoted errors are statistical, systematic, and theoretical respectively. These results are obtained by using five different form-factor calculations.

Contributed to the 31st International Conference on High Energy Physics,
7/24—7/31/2002, Amsterdam, The Netherlands

Stanford Linear Accelerator Center, Stanford University, Stanford, CA 94309

Work supported in part by Department of Energy contract DE-AC03-76SF00515.

The *BABAR* Collaboration,

B. Aubert, D. Boutigny, J.-M. Gaillard, A. Hicheur, Y. Karyotakis, J. P. Lees, P. Robbe, V. Tisserand, A. Zghiche

Laboratoire de Physique des Particules, F-74941 Annecy-le-Vieux, France

A. Palano, A. Pompili

Università di Bari, Dipartimento di Fisica and INFN, I-70126 Bari, Italy

J. C. Chen, N. D. Qi, G. Rong, P. Wang, Y. S. Zhu

Institute of High Energy Physics, Beijing 100039, China

G. Eigen, I. Ofte, B. Stugu

University of Bergen, Inst. of Physics, N-5007 Bergen, Norway

G. S. Abrams, A. W. Borgland, A. B. Breon, D. N. Brown, J. Button-Shafer, R. N. Cahn, E. Charles, M. S. Gill, A. V. Gritsan, Y. Groysman, R. G. Jacobsen, R. W. Kadel, J. Kadyk, L. T. Kerth, Yu. G. Kolomensky, J. F. Kral, C. LeClerc, M. E. Levi, G. Lynch, L. M. Mir, P. J. Oddone, T. J. Orimoto, M. Pripstein, N. A. Roe, A. Romosan, M. T. Ronan, V. G. Shelkov, A. V. Telnov, W. A. Wenzel

Lawrence Berkeley National Laboratory and University of California, Berkeley, CA 94720, USA

T. J. Harrison, C. M. Hawkes, D. J. Knowles, S. W. O'Neale, R. C. Penny, A. T. Watson, N. K. Watson

University of Birmingham, Birmingham, B15 2TT, United Kingdom

T. Deppermann, K. Goetzen, H. Koch, B. Lewandowski, K. Peters, H. Schmuecker, M. Steinke

Ruhr Universität Bochum, Institut für Experimentalphysik 1, D-44780 Bochum, Germany

N. R. Barlow, W. Bhimji, J. T. Boyd, N. Chevalier, P. J. Clark, W. N. Cottingham, C. Mackay, F. F. Wilson

University of Bristol, Bristol BS8 1TL, United Kingdom

K. Abe, C. Hearty, T. S. Mattison, J. A. McKenna, D. Thiessen

University of British Columbia, Vancouver, BC, Canada V6T 1Z1

S. Jolly, A. K. McKemey

Brunel University, Uxbridge, Middlesex UB8 3PH, United Kingdom

V. E. Blinov, A. D. Bukin, A. R. Buzykaev, V. B. Golubev, V. N. Ivanchenko, A. A. Korol, E. A. Kravchenko, A. P. Onuchin, S. I. Serednyakov, Yu. I. Skovpen, A. N. Yushkov

Budker Institute of Nuclear Physics, Novosibirsk 630090, Russia

D. Best, M. Chao, D. Kirkby, A. J. Lankford, M. Mandelkern, S. McMahon, D. P. Stoker

University of California at Irvine, Irvine, CA 92697, USA

C. Buchanan, S. Chun

University of California at Los Angeles, Los Angeles, CA 90024, USA

H. K. Hadavand, E. J. Hill, D. B. MacFarlane, H. Paar, S. Prell, Sh. Rahatlou, G. Raven, U. Schwanke, V. Sharma

University of California at San Diego, La Jolla, CA 92093, USA

J. W. Berryhill, C. Campagnari, B. Dahmes, P. A. Hart, N. Kuznetsova, S. L. Levy, O. Long, A. Lu, M. A. Mazur, J. D. Richman, W. Verkerke

University of California at Santa Barbara, Santa Barbara, CA 93106, USA

J. Beringer, A. M. Eisner, M. Grothe, C. A. Heusch, W. S. Lockman, T. Pulliam, T. Schalk, R. E. Schmitz, B. A. Schumm, A. Seiden, M. Turri, W. Walkowiak, D. C. Williams, M. G. Wilson

University of California at Santa Cruz, Institute for Particle Physics, Santa Cruz, CA 95064, USA

E. Chen, G. P. Dubois-Felsmann, A. Dvoretskii, D. G. Hitlin, F. C. Porter, A. Ryd, A. Samuel, S. Yang

California Institute of Technology, Pasadena, CA 91125, USA

S. Jayatilleke, G. Mancinelli, B. T. Meadows, M. D. Sokoloff

University of Cincinnati, Cincinnati, OH 45221, USA

T. Barillari, P. Bloom, W. T. Ford, U. Nauenberg, A. Olivas, P. Rankin, J. Roy, J. G. Smith, W. C. van Hoek, L. Zhang

University of Colorado, Boulder, CO 80309, USA

J. L. Harton, T. Hu, M. Krishnamurthy, A. Soffer, W. H. Toki, R. J. Wilson, J. Zhang

Colorado State University, Fort Collins, CO 80523, USA

D. Altenburg, T. Brandt, J. Brose, T. Colberg, M. Dickopp, R. S. Dubitzky, A. Hauke, E. Maly, R. Müller-Pfefferkorn, S. Otto, K. R. Schubert, R. Schwierz, B. Spaan, L. Wilden

Technische Universität Dresden, Institut für Kern- und Teilchenphysik, D-01062 Dresden, Germany

D. Bernard, G. R. Bonneaud, F. Brochard, J. Cohen-Tanugi, S. Ferrag, S. T'Jampens, Ch. Thiebaux, G. Vasileiadis, M. Verderi

Ecole Polytechnique, LLR, F-91128 Palaiseau, France

A. Anjomshoaa, R. Bernet, A. Khan, D. Lavin, F. Muheim, S. Playfer, J. E. Swain, J. Tinslay

University of Edinburgh, Edinburgh EH9 3JZ, United Kingdom

M. Falbo

Elon University, Elon University, NC 27244-2010, USA

C. Borean, C. Bozzi, L. Piemontese, A. Sarti

Università di Ferrara, Dipartimento di Fisica and INFN, I-44100 Ferrara, Italy

E. Treadwell

Florida A&M University, Tallahassee, FL 32307, USA

F. Anulli,[1] R. Baldini-Ferroli, A. Calcaterra, R. de Sangro, D. Falciai, G. Finocchiaro, P. Patteri, I. M. Peruzzi,[1] M. Piccolo, A. Zallo

Laboratori Nazionali di Frascati dell'INFN, I-00044 Frascati, Italy

S. Bagnasco, A. Buzzo, R. Contri, G. Crosetti, M. Lo Vetere, M. Macri, M. R. Monge, S. Passaggio, F. C. Pastore, C. Patrignani, E. Robutti, A. Santroni, S. Tosi

Università di Genova, Dipartimento di Fisica and INFN, I-16146 Genova, Italy

S. Bailey, M. Morii

Harvard University, Cambridge, MA 02138, USA

[1]Also with Università di Perugia, I-06100 Perugia, Italy

R. Bartoldus, G. J. Grenier, U. Mallik
University of Iowa, Iowa City, IA 52242, USA

J. Cochran, H. B. Crawley, J. Lamsa, W. T. Meyer, E. I. Rosenberg, J. Yi
Iowa State University, Ames, IA 50011-3160, USA

M. Davier, G. Grosdidier, A. Höcker, H. M. Lacker, S. Laplace, F. Le Diberder, V. Lepeltier, A. M. Lutz, T. C. Petersen, S. Plaszczynski, M. H. Schune, L. Tantot, S. Trincaz-Duvoid, G. Wormser
Laboratoire de l'Accélérateur Linéaire, F-91898 Orsay, France

R. M. Bionta, V. Brigljević , D. J. Lange, K. van Bibber, D. M. Wright
Lawrence Livermore National Laboratory, Livermore, CA 94550, USA

A. J. Bevan, J. R. Fry, E. Gabathuler, R. Gamet, M. George, M. Kay, D. J. Payne, R. J. Sloane, C. Touramanis
University of Liverpool, Liverpool L69 3BX, United Kingdom

M. L. Aspinwall, D. A. Bowerman, P. D. Dauncey, U. Egede, I. Eschrich, G. W. Morton, J. A. Nash, P. Sanders, D. Smith, G. P. Taylor
University of London, Imperial College, London, SW7 2BW, United Kingdom

J. J. Back, G. Bellodi, P. Dixon, P. F. Harrison, R. J. L. Potter, H. W. Shorthouse, P. Strother, P. B. Vidal
Queen Mary, University of London, E1 4NS, United Kingdom

G. Cowan, H. U. Flaecher, S. George, M. G. Green, A. Kurup, C. E. Marker, T. R. McMahon, S. Ricciardi, F. Salvatore, G. Vaitsas, M. A. Winter
University of London, Royal Holloway and Bedford New College, Egham, Surrey TW20 0EX, United Kingdom

D. Brown, C. L. Davis
University of Louisville, Louisville, KY 40292, USA

J. Allison, R. J. Barlow, A. C. Forti, F. Jackson, G. D. Lafferty, A. J. Lyon, N. Savvas, J. H. Weatherall, J. C. Williams
University of Manchester, Manchester M13 9PL, United Kingdom

A. Farbin, A. Jawahery, V. Lillard, D. A. Roberts, J. R. Schieck
University of Maryland, College Park, MD 20742, USA

G. Blaylock, C. Dallapiccola, K. T. Flood, S. S. Hertzbach, R. Kofler, V. B. Koptchev, T. B. Moore, H. Staengle, S. Willocq
University of Massachusetts, Amherst, MA 01003, USA

B. Brau, R. Cowan, G. Sciolla, F. Taylor, R. K. Yamamoto
Massachusetts Institute of Technology, Laboratory for Nuclear Science, Cambridge, MA 02139, USA

M. Milek, P. M. Patel
McGill University, Montréal, QC, Canada H3A 2T8

F. Palombo
Università di Milano, Dipartimento di Fisica and INFN, I-20133 Milano, Italy

J. M. Bauer, L. Cremaldi, V. Eschenburg, R. Kroeger, J. Reidy, D. A. Sanders, D. J. Summers
University of Mississippi, University, MS 38677, USA

C. Hast, P. Taras
Université de Montréal, Laboratoire René J. A. Lévesque, Montréal, QC, Canada H3C 3J7

H. Nicholson
Mount Holyoke College, South Hadley, MA 01075, USA

C. Cartaro, N. Cavallo, G. De Nardo, F. Fabozzi, C. Gatto, L. Lista, P. Paolucci, D. Piccolo, C. Sciacca
Università di Napoli Federico II, Dipartimento di Scienze Fisiche and INFN, I-80126, Napoli, Italy

J. M. LoSecco
University of Notre Dame, Notre Dame, IN 46556, USA

J. R. G. Alsmiller, T. A. Gabriel
Oak Ridge National Laboratory, Oak Ridge, TN 37831, USA

J. Brau, R. Frey, M. Iwasaki, C. T. Potter, N. B. Sinev, D. Strom, E. Torrence
University of Oregon, Eugene, OR 97403, USA

F. Colecchia, A. Dorigo, F. Galeazzi, M. Margoni, M. Morandin, M. Posocco, M. Rotondo, F. Simonetto, R. Stroili, C. Voci
Università di Padova, Dipartimento di Fisica and INFN, I-35131 Padova, Italy

M. Benayoun, H. Briand, J. Chauveau, P. David, Ch. de la Vaissière, L. Del Buono, O. Hamon, Ph. Leruste, J. Ocariz, M. Pivk, L. Roos, J. Stark
Universités Paris VI et VII, Lab de Physique Nucléaire H. E., F-75252 Paris, France

P. F. Manfredi, V. Re, V. Speziali
Università di Pavia, Dipartimento di Elettronica and INFN, I-27100 Pavia, Italy

L. Gladney, Q. H. Guo, J. Panetta
University of Pennsylvania, Philadelphia, PA 19104, USA

C. Angelini, G. Batignani, S. Bettarini, M. Bondioli, F. Bucci, G. Calderini, E. Campagna, M. Carpinelli, F. Forti, M. A. Giorgi, A. Lusiani, G. Marchiori, F. Martinez-Vidal, M. Morganti, N. Neri, E. Paoloni, M. Rama, G. Rizzo, F. Sandrelli, G. Triggiani, J. Walsh
Università di Pisa, Scuola Normale Superiore and INFN, I-56010 Pisa, Italy

M. Haire, D. Judd, K. Paick, L. Turnbull, D. E. Wagoner
Prairie View A&M University, Prairie View, TX 77446, USA

J. Albert, G. Cavoto,[2] N. Danielson, P. Elmer, C. Lu, V. Miftakov, J. Olsen, S. F. Schaffner, A. J. S. Smith, A. Tumanov, E. W. Varnes
Princeton University, Princeton, NJ 08544, USA

F. Bellini, D. del Re, R. Faccini,[3] F. Ferrarotto, F. Ferroni, E. Leonardi, M. A. Mazzoni, S. Morganti, G. Piredda, F. Safai Tehrani, M. Serra, C. Voena
Università di Roma La Sapienza, Dipartimento di Fisica and INFN, I-00185 Roma, Italy

[2]Also with Università di Roma La Sapienza, Roma, Italy
[3]Also with University of California at San Diego, La Jolla, CA 92093, USA

S. Christ, G. Wagner, R. Waldi

Universität Rostock, D-18051 Rostock, Germany

T. Adye, N. De Groot, B. Franek, N. I. Geddes, G. P. Gopal, S. M. Xella

Rutherford Appleton Laboratory, Chilton, Didcot, Oxon, OX11 0QX, United Kingdom

R. Aleksan, S. Emery, A. Gaidot, P.-F. Giraud, G. Hamel de Monchenault, W. Kozanecki, M. Langer, G. W. London, B. Mayer, G. Schott, B. Serfass, G. Vasseur, Ch. Yeche, M. Zito

DAPNIA, Commissariat à l'Energie Atomique/Saclay, F-91191 Gif-sur-Yvette, France

M. V. Purohit, A. W. Weidemann, F. X. Yumiceva

University of South Carolina, Columbia, SC 29208, USA

I. Adam, D. Aston, N. Berger, A. M. Boyarski, M. R. Convery, D. P. Coupal, D. Dong, J. Dorfan, W. Dunwoodie, R. C. Field, T. Glanzman, S. J. Gowdy, E. Grauges , T. Haas, T. Hadig, V. Halyo, T. Himel, T. Hryn'ova, M. E. Huffer, W. R. Innes, C. P. Jessop, M. H. Kelsey, P. Kim, M. L. Kocian, U. Langenegger, D. W. G. S. Leith, S. Luitz, V. Luth, H. L. Lynch, H. Marsiske, S. Menke, R. Messner, D. R. Muller, C. P. O'Grady, V. E. Ozcan, A. Perazzo, M. Perl, S. Petrak, H. Quinn, B. N. Ratcliff, S. H. Robertson, A. Roodman, A. A. Salnikov, T. Schietinger, R. H. Schindler, J. Schwiening, G. Simi, A. Snyder, A. Soha, S. M. Spanier, J. Stelzer, D. Su, M. K. Sullivan, H. A. Tanaka, J. Va'vra, S. R. Wagner, M. Weaver, A. J. R. Weinstein, W. J. Wisniewski, D. H. Wright, C. C. Young

Stanford Linear Accelerator Center, Stanford, CA 94309, USA

P. R. Burchat, C. H. Cheng, T. I. Meyer, C. Roat

Stanford University, Stanford, CA 94305-4060, USA

R. Henderson

TRIUMF, Vancouver, BC, Canada V6T 2A3

W. Bugg, H. Cohn

University of Tennessee, Knoxville, TN 37996, USA

J. M. Izen, I. Kitayama, X. C. Lou

University of Texas at Dallas, Richardson, TX 75083, USA

F. Bianchi, M. Bona, D. Gamba

Università di Torino, Dipartimento di Fisica Sperimentale and INFN, I-10125 Torino, Italy

L. Bosisio, G. Della Ricca, S. Dittongo, L. Lanceri, P. Poropat, L. Vitale, G. Vuagnin

Università di Trieste, Dipartimento di Fisica and INFN, I-34127 Trieste, Italy

R. S. Panvini

Vanderbilt University, Nashville, TN 37235, USA

S. W. Banerjee, C. M. Brown, D. Fortin, P. D. Jackson, R. Kowalewski, J. M. Roney

University of Victoria, Victoria, BC, Canada V8W 3P6

H. R. Band, S. Dasu, M. Datta, A. M. Eichenbaum, H. Hu, J. R. Johnson, R. Liu, F. Di Lodovico, A. Mohapatra, Y. Pan, R. Prepost, I. J. Scott, S. J. Sekula, J. H. von Wimmersperg-Toeller, J. Wu, S. L. Wu, Z. Yu

University of Wisconsin, Madison, WI 53706, USA

H. Neal

Yale University, New Haven, CT 06511, USA

1 Introduction

Exclusive $b \to u\ell\nu$ decays can be used to determine the modulus of V_{ub}, one of the smallest and least well known CKM matrix elements. Compared to the determination with inclusive decays, the extra kinematical constraints allow access to a larger part of the lepton-momentum spectrum, resulting in smaller extrapolation uncertainties. Experimentally, the main difficulty for the observation of $b \to u\ell\nu$ signal events is the large background from $b \to c\ell\nu$ events. Because $|V_{ub}/V_{cb}| \approx 0.1$, the branching fractions of the exclusive $b \to u\ell\nu$ decays ($\sim 10^{-4}$) are small compared to those of the charmed semileptonic decays, which are of the order of some percent.

To extract the branching fraction $B \to \rho e\nu$ and $|V_{ub}|$ requires use of hadronic form-factors which have to be obtained from theory. In this analysis we use five different form factor calculations: the two quark models ISGW2 [1] and Beyer/Melikhov [2], the lattice calculation by the UKQCD group [3], a model based on light cone sum rules (LCSR [4]), and a model based on heavy quark and $SU(3)$ symmetries (Ligeti/Wise [5]). The UKQCD and LCSR calculations directly use QCD, whereas the quark models are more phenomenological. All calculations use a particular value of $q^2 = (p_e + p_\nu)^2$ as a normalization point. Usually, $q^2_{\max}$ is used as this is the point where the hadronic system is least disturbed. The LCSR result however is normalized at a lower value of q^2.

2 The *BABAR* Detector and Data Set

The data used in this analysis were collected with the *BABAR* detector [6] at the PEP-II e^+e^- storage ring [7]. The integrated luminosity of the sample is $50.5\,\mathrm{fb}^{-1}$ taken at the $\Upsilon(4S)$ mass ("on-resonance"), corresponding to 55.2 million $B\bar{B}$ meson pairs. An additional $8.7\,\mathrm{fb}^{-1}$ of data were taken 40 MeV below the $\Upsilon(4S)$ resonance ("off-resonance").

PEP-II is an e^+e^- collider operated with asymmetric beam energies, producing a boosted ($\beta\gamma = 0.55$) $\Upsilon(4S)$ along the collision axis. *BABAR* is a solenoidal detector optimized for the asymmetric beam configuration at PEP-II. Charged particle (track) momenta are measured in a tracking system consisting of a 5-layer, double-sided, silicon vertex tracker (SVT) and a 40-layer drift chamber (DCH) filled with a gas mixture of helium and isobutane, both operating within a 1.5 T superconducting solenoidal magnet. Photon candidates are selected as local maxima of deposited energy in an electromagnetic calorimeter (EMC) consisting of 6580 CsI(Tl) crystals arranged in barrel and forward endcap subdetectors. Particle identification is performed by combining information from ionization measurements ($\mathrm{d}E/\mathrm{d}x$) in the SVT and DCH, and the Cherenkov angle θ_c measured by a detector of internally reflected Cherenkov light (DIRC). The DIRC system is a unique type of Cherenkov detector that relies on total internal reflection within the radiating volumes (quartz bars) to deliver the Cherenkov light outside the tracking and magnetic volumes, where the Cherenkov ring is imaged by an array of ~ 11000 photomultiplier tubes. The detector is surrounded by an instrumented flux-return (IFR).

3 Event Selection

In this section, we describe the selection of the exclusive semileptonic decays $B^+ \to \rho^0 e^+\nu$, $B^0 \to \rho^- e^+\nu$, $B^+ \to \omega e^+\nu$, $B^+ \to \pi^0 e^+\nu$, and $B^0 \to \pi^- e^+\nu$ (with $\rho^0 \to \pi^+\pi^-$, $\rho^\pm \to \pi^0\pi^\pm$ and $\omega \to \pi^0\pi^+\pi^-$). The charge conjugate decays are implied throughout. Our analysis strategy is similar to one used by CLEO [8]. The analysis is optimized for $B \to \rho e\nu$ decays; the π and

ω modes are included because of the crossfeeds into the ρ modes. Isospin and quark model relations are used to effectively measure only two branching fractions, one for $B \to \rho e\nu$ and one for $B \to \pi e\nu$. This is described in section 4. This analysis uses only electrons and not muons because the background contribution from fake leptons is much lower in the case of electrons. We reconstruct three kinematic variables which are used in the fit to extract the signal yields. These are the electron energy $E_{\rm lept}^{\rm CM}$, the invariant hadronic mass $M_{\pi\pi(\pi)}$ (for the ρ and ω modes), and the difference between the reconstructed and expected B meson energy ($\Delta E \equiv E_{\rm hadron} + E_\ell + |\vec{p}_{\rm miss}|c - E_{\rm beam}$) in the center-of-mass (CM) system.

Two electron energy regions are considered: $2.0 \leq E_{\rm lept}^{\rm CM} < 2.3$ GeV (LOLEP), and $2.3 \leq E_{\rm lept}^{\rm CM} < 2.7$ GeV (HILEP). The HILEP region is most sensitive to the signal because the $b \to ce\nu$ events are almost completely suppressed; the largest background source here is from continuum $e^+e^- \to q\bar{q}$ events. Real data taken below the $\Upsilon(4S)$ mass, which includes $e^+e^- \to e^+e^-(\gamma)$ events, is used for the continuum subtraction. In the LOLEP region, $b \to c$ decays dominate and provide the normalization of the background at higher electron energies.

Hadronic events are selected based on track multiplicity and event topology. The tracks must have at least 12 hits in the drift chamber. We also require that the impact parameter of the track along and transverse to the beam direction must be less than 3 cm and 1 cm, respectively. In addition, the transverse momentum must be greater than 0.1 GeV/c. Clusters in the electromagnetic calorimeter of *BABAR* that are not associated to any tracks must have an energy greater than 30 MeV to be considered as photons. In addition, the lateral moment of the shower energy distribution [10] must be smaller than 0.8. We select events with either $N_{\rm tracks} \geq 5$ or ($N_{\rm tracks} \geq 4$ and $N_{\rm photons} \geq 5$). The B mesons are produced nearly at rest so their decay products are distributed roughly uniformly in solid angle. In contrast, continuum events have a much more collimated (jet-like) event topology. They are suppressed by requiring the ratio of Fox-Wolfram moments H_2/H_0 [9] to be less than 0.4. This requirement suppresses 55% of the $e^+e^- \to q\bar{q}$ background and non-hadronic events, with a signal efficiency of 85%. In addition a neural net is used for further suppression of continuum events, as described below.

To identify electrons, we use a likelihood estimator, which uses information from several *BABAR* sub-detectors. The primary information is the ratio of the calorimeter energy to the track momentum. We require that the direction of the electron momentum is within the good calorimeter acceptance $-0.72 < \cos\theta_{e,{\rm lab}} < 0.92$. The efficiency of this selector is around 90%, with a pion misidentification rate of less than 0.1%. We also reject electrons from J/ψ decays (requiring two electrons identified with the likelihood electron selector and $3.00 < M_{e^+e^-} < 3.14$ GeV/c^2) and from photon conversions ($M_{e^+e^-} < 30$ MeV/c^2).

To reconstruct the neutral ρ meson we combine two oppositely charged tracks, and for the case of the charged ρ a track and a π^0. The π^0 mesons are reconstructed from two photons with an invariant mass $120 < M_{\gamma\gamma} < 145$ MeV/c^2 corresponding to $\pm 2\ \sigma$ from the nominal π^0 mass on average. To suppress combinatorial backgrounds we require that the pion with the highest momentum must have $p_\pi^{\rm CM} > 400$ MeV/c and the other pion must satisfy $p_\pi^{\rm CM} > 200$ MeV/c. For the ω, we combine two oppositely charged tracks with a π^0. The ω invariant mass is measured within ± 80 MeV/c^2 of the nominal ω mass [11]. This includes a side band region below and above the nominal ω mass. To suppress combinatorial backgrounds we require $p_\pi^{\rm CM} > 100$ MeV/c for each of the three pions. The charged tracks used to reconstruct the rho, $omega$, or $pi^\pm$ mesons must not have been identified as kaons.

In the following discussion all variables are taken in the center-of-mass frame. The neutrino

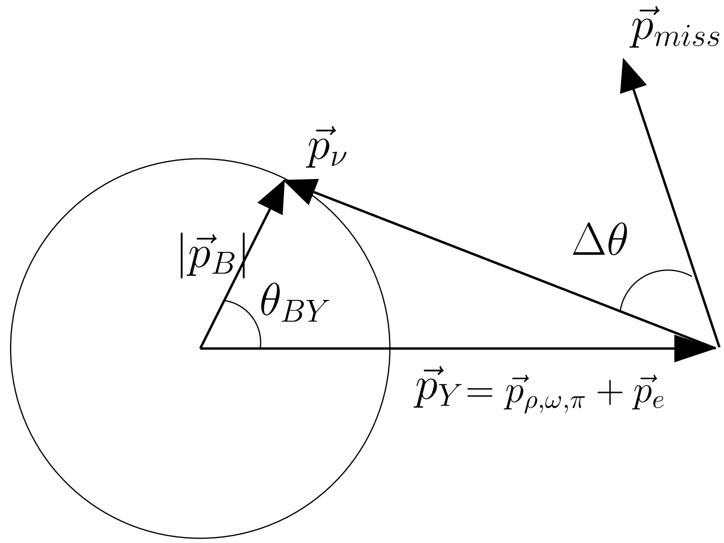

Figure 1: Angles θ_{BY} and $\Delta\theta$ defined in the $\Upsilon(4S)$ frame.

is reconstructed from the missing momentum:

$$\vec{p}_{\text{miss}} = -\sum_{\text{tracks}} \vec{p}_i - \sum_{\text{photons}} \vec{p}_i \ , \tag{1}$$

where the sums run over all reconstructed and accepted tracks and photons in the event. We then take $(E_\nu, \vec{p}_\nu) = (|\vec{p}_{\text{miss}}|c, \vec{p}_{\text{miss}})$.

A B-meson decay consistent with the signal modes is reconstructed using the constraints $E_B = E_{\text{beam}}$ and $(p_B - p_Y)^2 = 0$, where Y is the $(\rho,\ \omega,\ \pi) + e$ system. A useful quantity for testing consistency is the angle between the B momentum direction and that of the reconstructed Y system, see Fig. 1,

$$\cos\theta_{BY} = \frac{2E_B E_Y - (M_B^2 + M_Y^2)c^4}{2|\vec{p}_B||\vec{p}_Y|c^2} \ . \tag{2}$$

Background tends to have non-physical values of $\cos\theta_{BY}$. For the signal, small extensions of $|\cos\theta_{BY}| > 1$ are allowed because of detector resolution. We therefore require

$$|\cos\theta_{BY}| < 1.1 \ . \tag{3}$$

The efficiency of this requirement is almost 100% for the signal and it rejects more than 60% of the $b \to ce\nu$ and 80% of the continuum background.

We also compare the direction of the missing momentum $\vec{p}_{\text{miss}}$ with that of the neutrino momentum inferred from $\vec{p}_\nu = \vec{p}_B - \vec{p}_Y$. The latter is known to within an azimuthal ambiguity about the $\vec{p}_B$ direction because the magnitude, but not the direction, of the B meson momentum is known. We use the smallest possible angle $\Delta\theta_{\text{min}}$ between the two directions, which is obtained when the momenta of $\vec{p}_Y$, $\vec{p}_\nu$, and $\vec{p}_{\text{miss}}$ are in the same plane, see Fig. 1. We use the requirement

$$0.8 < \cos\Delta\theta_{\text{min}} \leq 1.0 \ . \tag{4}$$

This has been optimized using a Monte Carlo simulation, in such a way as to minimize the relative error on the measured branching fraction.

In addition, we require $|\cos\theta_{\rm miss}| < 0.9$ where $\theta_{\rm miss}$ is the angle between $\vec{p}_{\rm miss}$ and the beam axis. This cut rejects events with missing high momentum particles close to the beam axis.

The continuum $e^+e^- \to q\bar{q}$, where $q = u, d, s, c$, is an important background at high electron energies, where we are most sensitive to the signal. To reject these events, we use a neural net with 14 event shape variables such as the track and cluster energies in nine cones around the electron-momentum axis. The optimized cut on the neural net output suppresses more than 90% of the continuum, after all other requirements have been applied, in the HILEP region. The selection efficiency on the signal is 60%.

After all the above criteria, there can still be several candidates per event. This follows from the large width of the ρ and also because we are reconstructing five different decay modes. To avoid statistical difficulties related to large numbers of combinations, we choose one candidate per event, namely the one with a reconstructed total momentum closest to the B meson momentum:

$$|\vec{p}_{\rm hadron} + \vec{p}_e + \vec{p}_{\rm miss}| \;\text{ closest to }\; |\vec{p}_B|. \tag{5}$$

The efficiency of this selection for the signal is close to 85% .

At each step of the selection procedure the data distributions agree well with their Monte Carlo simulation.

The total efficiencies in the HILEP region are 4.21% for the $B^+ \to \rho^0 e^+\nu$ mode and 3.31% for the $B^0 \to \rho^- e^+\nu$ mode. These efficiencies are determined using the ISGW2 form-factors. They are defined here as the number of HILEP signal events that pass all selection criteria and are reconstructed in the specified channel divided by the number of all generated events (of all electron momenta) for this channel. The signal and crossfeed efficiencies for all channels are listed in Table 1.

Table 1: Selection efficiencies for the modes $B^+ \to \rho^0 e^+\nu$, $B^0 \to \rho^- e^+\nu$, $B^+ \to \omega e^+\nu$, $B^+ \to \pi^0 e^+\nu$, and $B^0 \to \pi^- e^+\nu$ in the HILEP region. These efficiencies have been determined using simulated data (ISGW2 model). They are defined as the number of selected events passing all cuts divided by the number of all generated events (in the full lepton energy range) for the specified channel.

	Reconstruction Efficiency (%)				
Generated	$B^+ \to \rho^0 e^+\nu$	$B^0 \to \rho^- e^+\nu$	$B^+ \to \omega e^+\nu$	$B^+ \to \pi^0 e^+\nu$	$B^0 \to \pi^- e^+\nu$
$B^+ \to \rho^0 e^+\nu$	4.21	0.99	0.30	0.58	1.35
$B^0 \to \rho^- e^+\nu$	1.04	3.31	0.31	1.08	1.32
$B^+ \to \omega e^+\nu$	1.97	1.55	1.57	0.94	0.88
$B^+ \to \pi^0 e^+\nu$	0.23	0.41	0.07	1.28	0.40
$B^0 \to \pi^- e^+\nu$	0.42	0.47	0.05	0.33	1.63

4 Fit Method

We have performed a binned maximum-likelihood fit of the two-dimensional distribution ($M_{\pi\pi(\pi)}$, ΔE) simultaneously in the two electron energy ranges (LOLEP, HILEP) and the decay modes $B^+ \to \rho^0 e^+\nu$, $B^0 \to \rho^- e^+\nu$, and $B^+ \to \omega e^+\nu$. For the $B \to \rho e\nu$ modes, the data are divided into 10×10 bins over the ($M_{\pi\pi}$, ΔE) region $0.25 \leq M_{\pi\pi} \leq 2.00$ GeV/c^2 and $|\Delta E| \leq 2$ GeV. The bin size for the fit is thus 175 MeV/c^2 in $M_{\pi\pi}$ and 400 MeV in ΔE. For the ω channel, we use 5 bins in the range 782 ± 80 MeV/c^2 and 10 bins in $|\Delta E| \leq 2$ GeV. The modes $B^+ \to \pi^0 e^+ \nu$ and $B^0 \to \pi^- e^+ \nu$ are also included to model the crossfeeds into the other signal channels; for these modes only ΔE is used as a fit variable.

Our fit includes contributions from the signal modes, other $b \to ue\nu$ decays, $b \to ce\nu$ decays, continuum, and a contribution from misidentified electrons. For the signal and backgrounds coming from other $b \to ue\nu$ and $b \to ce\nu$ decays, Monte Carlo simulation provides the shapes of the distributions. The decays $B \to D^* \ell \nu$ have been simulated using heavy quark effective theory (HQET [12]). The modes $B \to D^* \pi \ell \nu$ are simulated according to the Goity-Roberts model [13]. Resonant $b \to u \ell \nu$ downfeed modes are implemented according to the ISGW2 model. Non-resonant $b \to u \ell \nu$ modes are implemented according to a model by Fazio and Neubert [14].

Isospin and quark model relations are used to constrain the relative normalizations of $B^0 \to \rho^- e^+ \nu$, $B^+ \to \rho^0 e^+ \nu$, and $B^+ \to \omega e^+ \nu$ and therefore to reduce the number of free fit parameters:

$$\Gamma(B^0 \to \rho^- e^+ \nu) = 2\Gamma(B^+ \to \rho^0 e^+ \nu), \tag{6}$$

$$\Gamma(B^+ \to \rho^0 e^+ \nu) = \Gamma(B^+ \to \omega e^+ \nu), \tag{7}$$

$$\Gamma(B^0 \to \pi^- e^+ \nu) = 2\Gamma(B^+ \to \pi^0 e^+ \nu). \tag{8}$$

Isospin breaking effects are discussed in [15] and [16]. We assume that the isospin relations in Eqs. 6 and 7 are broken by not more than 3%. This would have a negligible effect on our result and therefore we do not include a corresponding systematic error. The isospin relations were tested experimentally. We find that the isospin relations Eqs. 6 and 7 are consistent with the data within 1.3 σ and 1.7 σ.

We use the following 9 free parameters for the fit:

- $\mathcal{B}(B^0 \to \rho^- e^+ \nu)$ (1 parameter);
- $\mathcal{B}(B^0 \to \pi^- e^+ \nu)$ (1 parameter);
- the scale factors of the $b \to ue\nu$ background in each electron energy bin (2 parameters), that give the overall normalization of all $b \to ue\nu$ modes that are not signal modes, relative to that expected from the Monte Carlo simulation;
- the scale factors, one for each mode, that give the overall normalization of the $b \to ce\nu$ background relative to that expected from the Monte Carlo simulation (5 parameters).

The maximum-likelihood fit method used in this analysis has been described in [17]. The fit takes into account the statistical fluctuations not only of the on-resonance and off-resonance data but also those of the Monte Carlo contributions. We have performed a toy Monte Carlo check to verify the stability of the fit method and to check the statistical error returned by the fit.

Whereas the signal modes $B^+ \to \rho^0 e^+ \nu$, $B^0 \to \rho^- e^+ \nu$, and $B^+ \to \omega e^+ \nu$ are simulated with five different form-factors, all other $b \to ue\nu$ modes (downfeed background) are simulated using the ISGW2 form-factor only.

5 Fit Results

The signal yields extracted from the binned maximum-likelihood fit in the HILEP region are 324 ± 40 $B^+ \to \rho^0 e^+ \nu$ events and 510 ± 63 $B^0 \to \rho^- e^+ \nu$ events, based on the ISGW2 calculation. The composition of events for the $B^0 \to \rho^- e \nu$ and $B^+ \to \rho^0 e^+ \nu$ channel is shown in Table 2. The isospin-constrained results for the five different form-factors are shown in Fig. 2. A

Table 2: Summary of data yields for the $B^0 \to \rho^- e^+ \nu$ and $B^+ \to \rho^0 e^+ \nu$ modes with electron energies between 2.3 and 2.7 GeV (HILEP), and between 2.0 and 2.3 GeV (LOLEP). The yields presented in this table were obtained using the ISGW2 form-factor. The downfeed background includes all $B \to X_u e\nu$ modes except for ρ, ω, and π. The crossfeed signal contribution corresponds to events from the other signal modes with ρ^0, ω, or π and is constrained to the signal in the fit. All errors are statistical only.

	$B^0 \to \rho^- e^+ \nu$		$B^+ \to \rho^0 e^+ \nu$	
	HILEP	LOLEP	HILEP	LOLEP
On-resonance yield	2302	39349	2213	40155
Direct signal	510 ± 63	718 ± 89	324 ± 40	440 ± 55
Crossfeed signal	262 ± 32	538 ± 73	363 ± 42	725 ± 86
Downfeed	203 ± 55	2278 ± 403	226 ± 92	2435 ± 430
$b \to ce\nu$	414 ± 5	33859 ± 438	367 ± 5	34366 ± 458
$e^+e^- \to q\bar{q}$	917 ± 73	1928 ± 106	912 ± 73	2063 ± 110
Fake electrons	12 ± 3	80 ± 9	18 ± 4	76 ± 9

χ^2 test has been performed to check the quality of the fit. Bins in sparsely populated regions have been combined before the χ^2 calculation. For ISGW2, we obtain $\chi^2 = 91$ for $N_{\rm dof} = 93$, which corresponds to a p-value of 0.52, and similarly good fit quality for the other four form-factor calculations.

The five fit parameters describing the $b \to c$ backgrounds agree with the Monte Carlo expectations within 9% on average. The two parameters describing the $b \to u$ downfeed background in LOLEP and HILEP agree to better than 1.5 σ and 1.2 σ. The fit result for the π modes is $\mathcal{B}(B^0 \to \pi^- e^+ \nu) = (1.87 \pm 0.56) \times 10^{-4}$ for the ISGW2 calculation.

The projections of the ISGW2 fit result for the two electron energy bins after subtraction of the continuum contribution are shown in Figs. 3 and 4. Good agreement between the data and fit result is seen in each of these figures. The fits for the other four form-factor calculations show similar agreement.

6 Systematic Errors

The summary of all systematic errors on the branching fraction that have been considered is shown in Table 3. The total systematic error is taken as the quadratic sum of all individual errors. The fluctuations due to finite Monte Carlo statistics are included in the statistical error and not in the systematic error.

The largest single systematic error comes from the uncertainty in the shape of the downfeed background. We use the ISGW2 model to describe resonant downfeed modes, and a model by Fazio and Neubert [14] for non-resonant modes. The fraction of non-resonant events in the downfeed background is varied from 0% to 68% to estimate this systematic uncertainty. The composition of the resonant $b \to u$ downfeed component has been varied by changing the branching fraction for individual resonances by $\pm 50\%$, and keeping the total rate constant.

We have also varied the most important selection requirements of this analysis within a reasonable range and have changed our fit method (fitting with only four channels, or without the LOLEP region, or with different binnings). Most variations seen are within 1σ of the expected

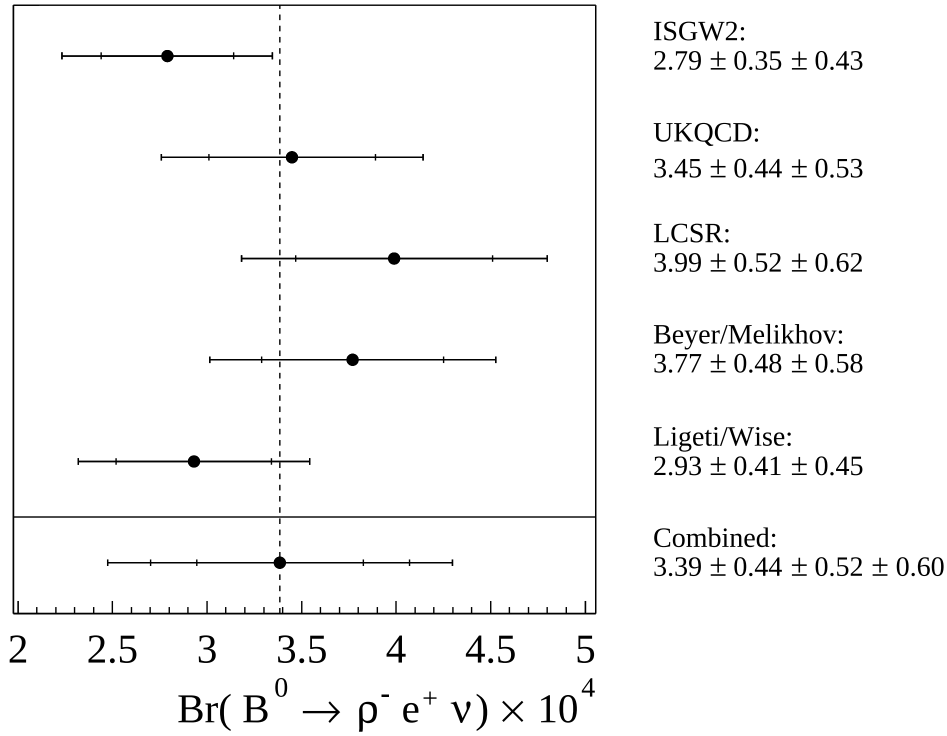

Figure 2: The $B^0 \to \rho^- e^+ \nu$ branching fraction results using the ISGW2, UKQCD, LCSR, Beyer/Melikhov, and Ligeti/Wise form-factors. The errors shown are statistical, systematic, and (only in case of the combined result) theoretical, successively combined in quadrature. The combined central value is determined by taking the unweighted mean of all form-factor results. The statistical and systematic errors of the combined result are determined by taking the means of the relative errors of each individual result, and its theoretical error is taken to be one half of the full spread of the results.

statistical variation, some are close to 2σ. To be conservative we assign a systematic error corresponding to half the largest variations seen. This corresponds to the last two systematic errors quoted in Table 3.

7 Extraction of $|V_{ub}|$

The CKM matrix element $|V_{ub}|$ can be obtained from the branching fraction $\mathcal{B}(B^0 \to \rho^- e^+ \nu)$ using

$$|V_{ub}| = \sqrt{\frac{\mathcal{B}(B^0 \to \rho^- e^+ \nu)}{\tilde{\Gamma}_{\rm thy} \tau_{B^0}}}\,, \tag{9}$$

where $\tilde{\Gamma}_{\rm thy}$ is the predicted form-factor normalization. Values of $\tilde{\Gamma}_{\rm thy}$ and theoretical errors for each form-factor calculation are given in Table 4. The calculations quote errors on $\tilde{\Gamma}_{\rm thy}$ between 15% and 50%. We use $\tau_{B^0} = 1.548 \pm 0.032$ ps [11], and the branching fractions are taken separately for each form-factor as listed in Fig. 2. The combined central value is determined by taking the weighted mean of all form-factor results. The statistical and systematic errors of the

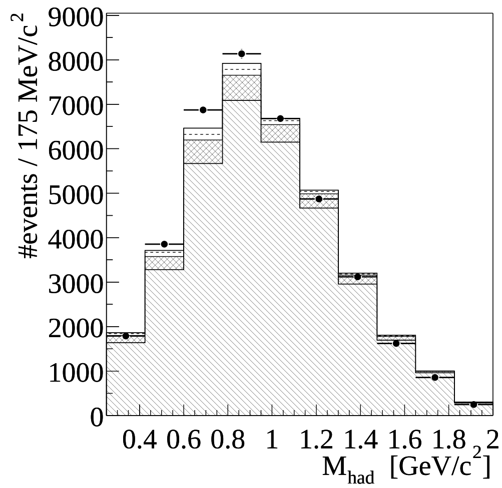

(a) $M_{\pi\pi}$ (LOLEP)

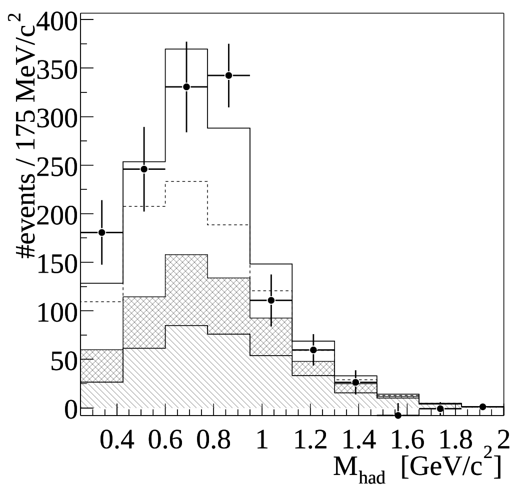

(b) $M_{\pi\pi}$ (HILEP)

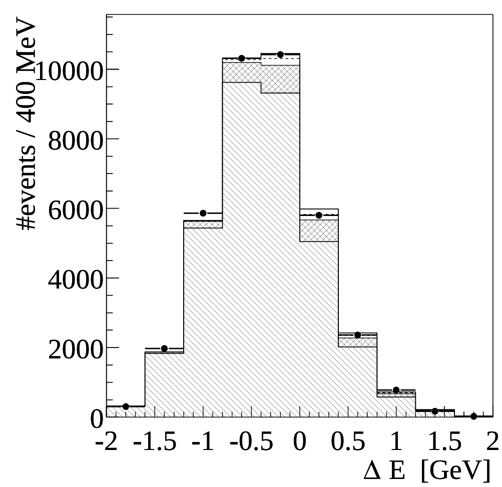

(c) ΔE (LOLEP)

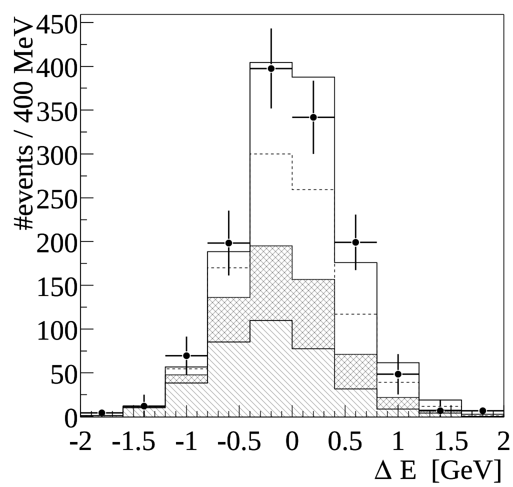

(d) ΔE (HILEP)

Figure 3: Continuum-subtracted projections of the ISGW2 fit result for the $B^+ \to \rho^0 e^+ \nu$ channels in the LOLEP and HILEP electron energy regions; the contributions are the direct and crossfeed components of the signal (unhatched region, above and below the dashed line, respectively); the background from $b \to u e \nu$ other than $B \to \rho e \nu$ and $B \to \omega e \nu$ modes (double-hatched region); the background from $b \to c e \nu$ and other backgrounds (single-hatched region).

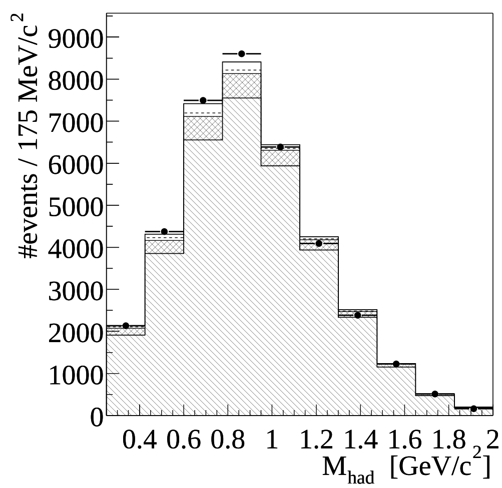

(a) $M_{\pi\pi}$ (LOLEP)

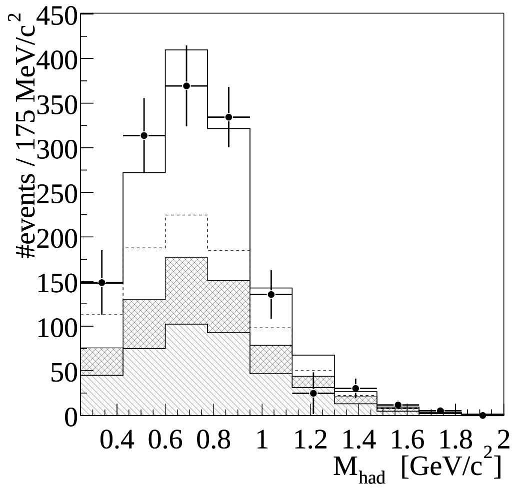

(b) $M_{\pi\pi}$ (HILEP)

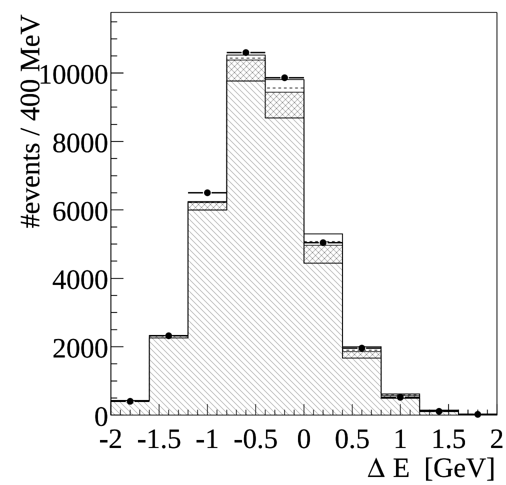

(c) ΔE (LOLEP)

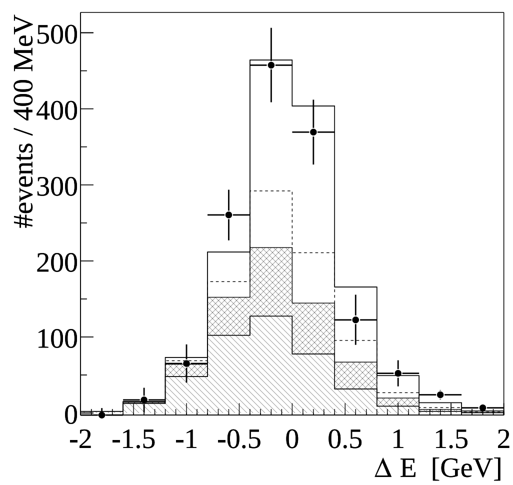

(d) ΔE (HILEP)

Figure 4: Continuum-subtracted projections of the ISGW2 fit result for the $B^0 \rightarrow \rho^- e^+ \nu$ channels in the LOLEP and HILEP electron energy regions; the contributions are the direct and crossfeed components of the signal (unhatched region, above and below the dashed line, respectively); the background from $b \rightarrow ue\nu$ other than $B \rightarrow \rho e\nu$ and $B \rightarrow \omega e\nu$ modes (double-hatched region); the background from $b \rightarrow ce\nu$ and other backgrounds (single-hatched region).

Table 3: Summary of all contributions to the systematic error on the branching fraction for $B \to \rho e \nu$.

Error contribution	$\delta\mathcal{B}_\rho/\mathcal{B}_\rho$ (%)
Tracking Efficiency	± 5
Tracking Resolution	± 1
Photon/π^0 Efficiency	± 5
Photon/π^0 Energy Scale	± 3
$b \to c$ Background Composition	$^{+1.4}_{-1.7}$
Resonant $b \to u$ Background Composition	$^{+6}_{-4}$
Non-Resonant $b \to u$ Background	± 9
B Lifetime	± 1
B Counting	± 1.6
Fake Electrons	$< \pm 1$
Electron Id	± 2
$f_{\pm}/f_{00}$	$< \pm 1$
Data Selection	± 6
Fit Method	$^{+4}_{-6}$
Total Systematic Error	± 15.5

Table 4: $\tilde{\Gamma}_{\rm thy}$ predicted by various form-factor calculations.

Form-factor	$\tilde{\Gamma}_{\rm thy}$ (ps^{-1})	Estimated error on $\tilde{\Gamma}_{\rm thy}$(%)
ISGW2	14.2	± 50
LCSR	16.9	± 32
UKQCD	16.5	$^{+21}_{-14}$
Beyer/Melikhov	16.0	± 15
Ligeti/Wise	19.4	± 29

final combined result are determined by taking the mean of the relative errors of each individual result. The theoretical error is taken to be one half of the full spread of all fit results (including theoretical errors). The results for each form-factor and the combined result is shown in Fig. 5.

A comparison of our preliminary result with inclusive and exclusive measurements from CLEO and the inclusive measurement from LEP is shown in Fig. 6. Two exclusive results from CLEO are quoted. The first result is obtained from an analysis very similar to the analysis presented here [8], the second result is an average of their first result and a separate analysis [8, 18]. Our result is compatible with all other measurements within errors and lies between the CLEO and LEP results.

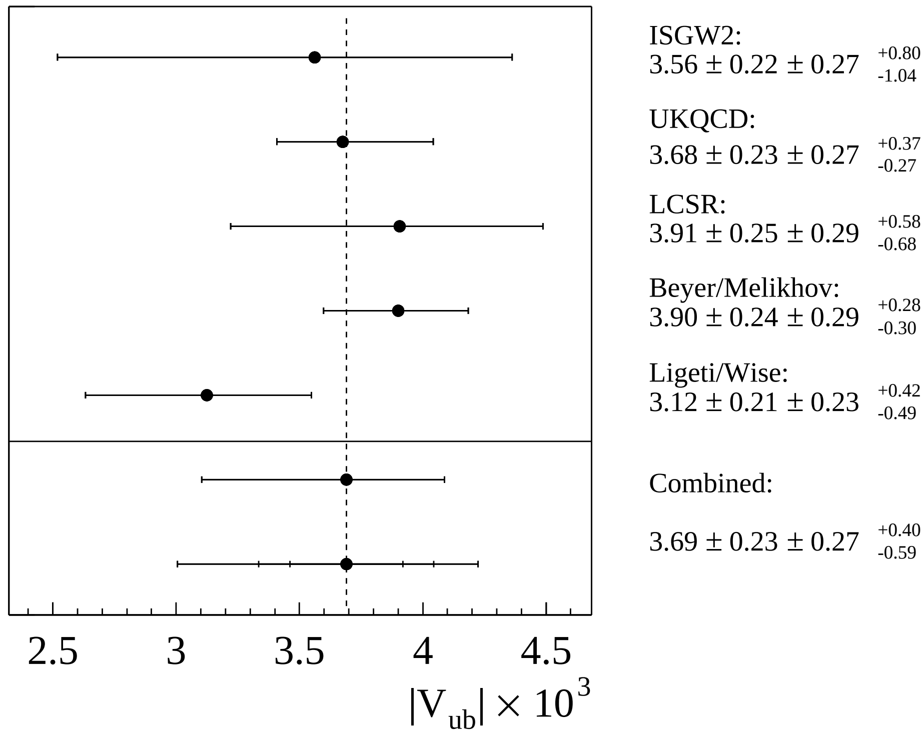

Figure 5: $|V_{ub}|$ determined using the ISGW2, UKQCD, LCSR, Beyer/Melikhov, and Ligeti/Wise form-factors. The results for each form-factor are drawn with theoretical error bars only. The combined central value is determined by taking the mean of all form-factor results, weighted by their individual theoretical error. The theoretical error of the combined result is taken to be one half of the full spread of results, including the errors. The combined result is also drawn with statistical, systematic, and theoretical errors successively added in quadrature. The statistical and systematic errors of the combined result are determined by taking the mean of the relative errors of each individual result. In addition we give, on the right side of the figure, all five results with their statistical, systematic, and theoretical errors.

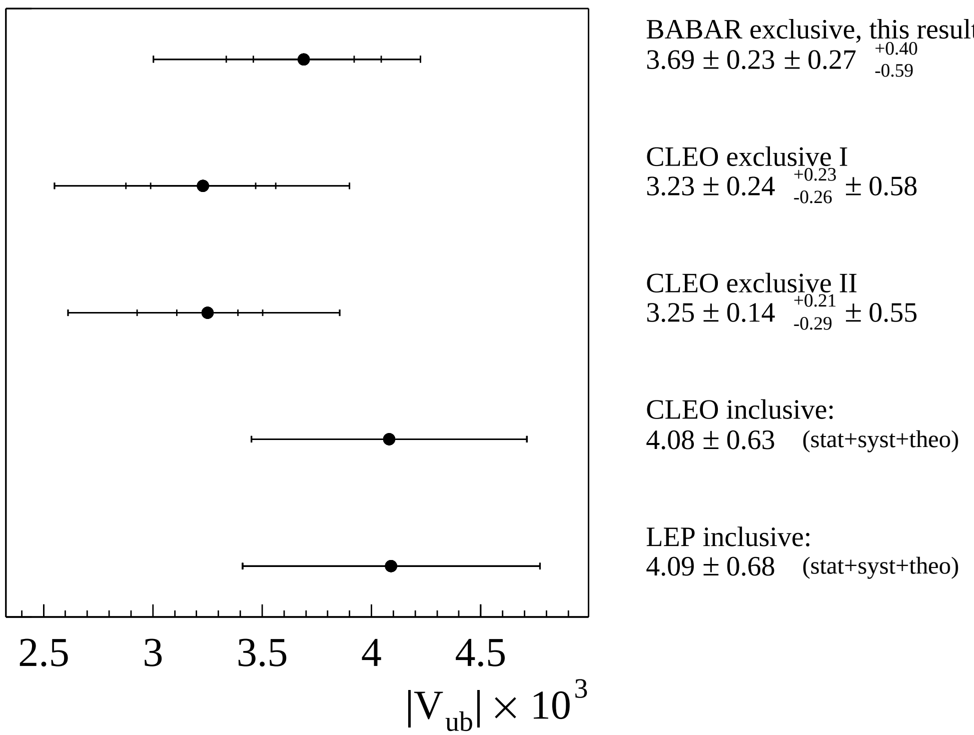

Figure 6: Comparison with results from other experiments. The CLEO exclusive I result [8] is obtained from an analysis very similar to the analysis presented here, their exclusive II result [18] is an average of the exclusive I result and a separate CLEO result.

8 Acknowledgements

We are grateful for the extraordinary contributions of our PEP-II colleagues in achieving the excellent luminosity and machine conditions that have made this work possible. The success of this project also relies critically on the expertise and dedication of the computing organizations that support *BABAR*. The collaborating institutions wish to thank SLAC for its support and the kind hospitality extended to them. This work is supported by the US Department of Energy and National Science Foundation, the Natural Sciences and Engineering Research Council (Canada), Institute of High Energy Physics (China), the Commissariat à l'Energie Atomique and Institut National de Physique Nucléaire et de Physique des Particules (France), the Bundesministerium für Bildung und Forschung and Deutsche Forschungsgemeinschaft (Germany), the Istituto Nazionale di Fisica Nucleare (Italy), the Research Council of Norway, the Ministry of Science and Technology of the Russian Federation, and the Particle Physics and Astronomy Research Council (United Kingdom). Individuals have received support from the A. P. Sloan Foundation, the Research Corporation, and the Alexander von Humboldt Foundation.

References

[1] D. Scora and N. Isgur, CEBAF Preprint No. CEBAF-TH-94-14.

[2] M. Beyer and D. Melikhov, *Phys. Lett.* **B436**, 344 (1998).

[3] L. Del Debbio *et al.*, *Phys. Lett.* **B 416**, 392 (1998).

[4] P. Ball and V.M. Braun, *Phys. Rev.* **D58**, 094016 (1998).

[5] Z. Ligeti and M.B. Wise, *Phys. Rev.* **D53**, 4937 (1996).

[6] BABAR Collaboration, B. Aubert *et al.*, *Nucl. Instr. and Methods* **A479**, 1 (2002).

[7] PEP II, SLAC-418, LBL-5379 (1993).

[8] CLEO Collaboration, B.H. Behrens *et al.*, *Phys. Rev.* **D61**, 052001 (2000).

[9] G.C. Fox and S. Wolfram, *Nucl. Phys.* **B149**, 413 (1979).

[10] A. Drescher *et al.*, *Nucl. Instr. and Meth.* **A237**, 464 (1985).

[11] Particle Data Group, D.E. Groom *et al.*, Eur. Phys. Jour. C **15**, 1 (2000).

[12] I.I. Bigi, M. Shifman, and N.G. Uraltsev, *Annu. Rec. Nucl. Part. Sci.* **47**, 591 (1997).

[13] J.L. Goity and W. Roberts, Phys. Rev. **D51**, 3459 (1995).

[14] F. Fazio and M. Neubert, $B \to X_u \ell \nu$ *decay distributions to order* α_s, hep-ph/9905351v2.

[15] J.L. Diaz-Cruz, G. Lopez Castro and J.H. Munoz, Phys. Rev. **D54**, 2388 (1996).

[16] D.J. Lange, *Rare exclusive semileptonic decays at CLEO*, Ph.D. Thesis, University of California, Santa Barbara (1999).

[17] R.J. Barlow and C. Beeston, *Comp. Phys. Comm.* **77**, 219 (1993).

[18] J.P. Alexander *et al.*, *Phys. Rev. Lett.* **77**, 5000 (1996).